

## Supplementary Information for

### A Homogeneous Atomic Layer $\text{MoS}_{2(1-x)}\text{Se}_{2x}$ Alloy Prepared by Low-Pressure Chemical Vapor Deposition, and its Properties

Sima Umra<sup>a</sup>, Jaeho Jeon<sup>a</sup>, Su Min Jeon<sup>a</sup>, Young Jin Choi<sup>b\*</sup>, and Sungjoo Lee<sup>a,c\*</sup>

<sup>a</sup>SKKU Advanced Institute of Nanotechnology (SAINT), Sungkyunkwan University (SSKU), Suwon 440-746, Korea. E-mail: [leesj@skku.edu](mailto:leesj@skku.edu)

<sup>b</sup>Department of Nanotechnology and Advanced Materials Engineering, Sejong University, Seoul 143-747, Korea

<sup>c</sup>School of Electronics and Electric Engineering, Sungkyunkwan University (SKKU), Suwon 440-746, Korea.

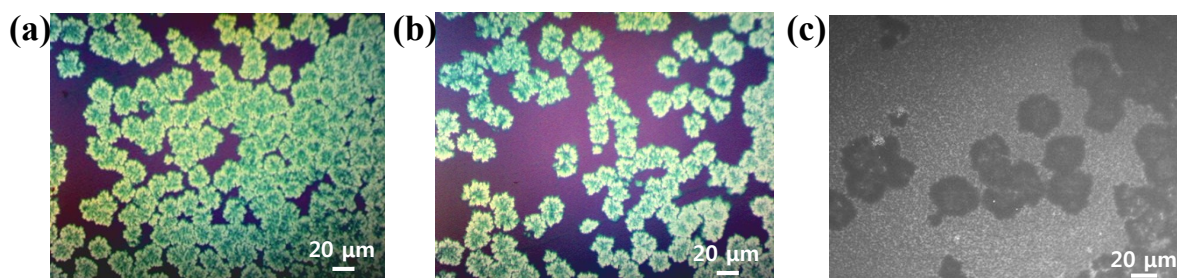


**Figure S1.** OM images (a-b) and SEM image (c) of  $\text{MoS}_{2(1-x)}\text{Se}_{2x}$  alloy that grew in a uniform flower-like shape on the whole substrate when  $\text{MoO}_3$  powder was spread in a uniform layer on the alumina boat.

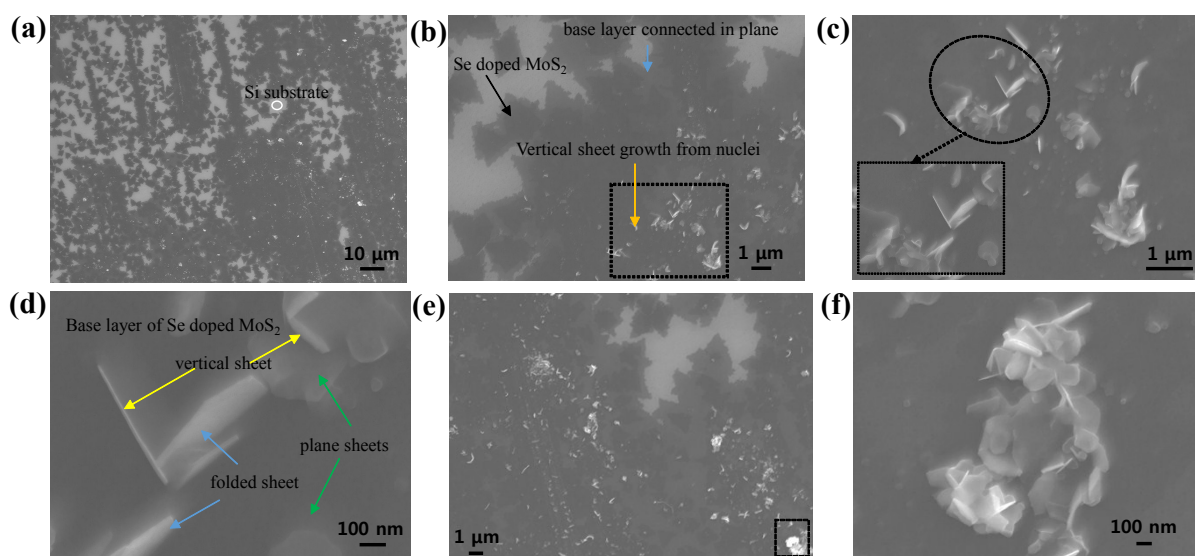


**Figure S2.** SEM images of an as-grown  $\text{MoS}_{2(1-x)}\text{Se}_{2x}$  alloy from substrate A. The images clearly show that the growth of vertical sheet when two or more domains merge to each other.

**Growth mechanism.** Thermodynamically, nucleation for crystal growth depends on the chemical potential and activation free energy of the surface and interface.<sup>S1</sup> During crystallization, crystal growth onto the stable nuclei proceeds until supersaturation is relieved. Based on the kinetic theory of two-dimensional nucleation,<sup>S1, S2</sup> the rate of formation of stable two-dimensional nuclei is generally described by equation 2 in the main text. It is clear that the surface energy and MoO<sub>3</sub> precursor concentration are involved in the nucleation and growth of films, and can be analyzed to provide information for manipulating the film growth model during the deposition process. Gibbs thermodynamic treatment of nucleation gives the free energy changes, as below:<sup>S3</sup>

$$\Delta F^* = -n\Delta\mu + \gamma_{nv} A \quad (\text{S1})$$

where n is the number of molecules in the nucleus,  $\Delta\mu$  is the chemical potential difference between the vapor and the film nucleus which defines supersaturation,  $\gamma_{nv}$  is the surface tension between the nucleus and the surrounding vapor, A is the surface area of the nucleus, and  $v_c$  denotes the molecular volume of the new solid phase. During the nucleation process, the system can be thought of as being in an equilibrium condition (**Fig. 2b**) described by Young's equation, below, which explains the interfacial tension between the two phases (film as nucleus and substrate) during vapor deposition:

$$\gamma_{sv} = \gamma_{ns} + \gamma_{nv} \cos \theta \quad (\text{S2})$$

$$\text{or} \quad \cos \theta = \frac{[\gamma_{sv} - \gamma_{ns}]}{\gamma_{nv}} \quad (\text{S3})$$

where  $\gamma_{sv}$  is substrate-vapor interfacial energy,  $\gamma_{ns}$  is film-substrate interfacial energy,  $\gamma_{nv}$  is film-vapor interfacial energy, and  $\theta$  is wetting angle. Then, equation (S1), as given below, applies for circular cap-shaped nuclei:

$$\Delta F^* = -\frac{4}{3v_c} \pi r^3 \Delta\mu \left\{ \frac{2 - 3\cos \theta + \cos^3 \theta}{4} \right\} + 4 \left\{ \frac{1 - \cos \theta}{2} \right\} \pi r^2 \gamma_{nv} + \pi r^2 \sin^2 \theta (\gamma_{ns} - \gamma_{sv}) \quad (\text{S4})$$

Using Young's equation (S3) and equation (S4) gives the following:

$$\Delta F^* = -\frac{4}{3v_c} \pi r^3 \Delta\mu f(\theta) + 4f(\theta) \pi r^2 \gamma_{nv} \quad (\text{S5})$$

$$\text{where } f(\theta) = \frac{2 - 3\cos\theta + \cos^3\theta}{4}$$

For stable nuclei, free energy will reach a maximum at a critical nuclear radius ( $r^* \sim 2\gamma^{uv}/\Delta\mu$ ) and a nucleus will start to grow in a stable structure by adatom impingement. Then, Gibbs free energy at the critical radius is:

$$\Delta F^* = \frac{16\pi\gamma_{nv}^3 v_c^2}{3\Delta\mu^2} f(\theta) \quad (\text{S6})$$

The above kinetic study reveals that MoO<sub>3</sub> precursor concentration and corresponding interface energy can play effective roles in nucleation and growth. For island growth,  $\theta > 0$ , therefore  $\gamma_{sv} < \gamma_{ns} + \gamma_{nv}$  and growth follows the Volmer–Weber (island) growth mode. For Stranski–Krastanov growth, initially  $\gamma_{sv} \geq \gamma_{ns} + \gamma_{nv}$  is satisfied, leading to layer-by layer growth when  $\theta > 0$ , but the buildup of strain energy from the lattice mismatch between the film and the substrate can lead the growth transformation into island-like growth after a few layers. **Figure S2** clearly shows the growth of an alloy following the SK model for a stable structure.

Name	At. (%)		
	Position A	Position B	Position C
<b>Se 3d</b>	1.77	2.14	1.55
<b>S 2p</b>	63.28	36.36	32.41
<b>Mo 3d</b>	23.21	18.57	13.37
<b>O 1s</b>	11.75	42.93	52.67

**Table S1.** Atomic weight % composition of a MoS<sub>2(1-x)</sub>Se<sub>2x</sub> alloy.

**Manifestation of oxygen level:** XPS analysis by XPS survey and core level spectra of the composition of MoS<sub>2(1-x)</sub>Se<sub>2x</sub> alloys were studied for all synthesized alloys A, B, and C. The oxidation of Mo atoms at the edge sites is prominent, as demonstrated by the Mo 3d core level spectra. We have deconvoluted the O 1s core level spectra with the best-fit parameter ( $R^2 \sim 0.99$ ) into peaks centered at

~532.1 eV, ~530.3 eV, and 529.8 eV corresponds to Si-O bonding, Mo<sup>+6</sup>-O, and Mo<sup>+4</sup>-O bonding, respectively. In the case of molybdenum oxide, the binding energy is flexible because of a varying number of bound oxygen atoms.<sup>S4</sup> In all O1s spectra, a small peak is present, which corresponds to Mo<sup>+4</sup>-O, confirming the presence of a very small amount of MoO<sub>2</sub>. However, in the case of the third sample, along with the Mo<sup>+4</sup>-O peak, one more peak with higher binding energy of small intensity is evident, corresponding to Mo<sup>+6</sup>-O. The very low contribution of Mo<sup>+4</sup>-O and the absence of Mo<sup>+6</sup>-O in the 2 other samples showcases the pure crystallinity of the MoS<sub>2(1-x)</sub>Se<sub>2x</sub> alloys.

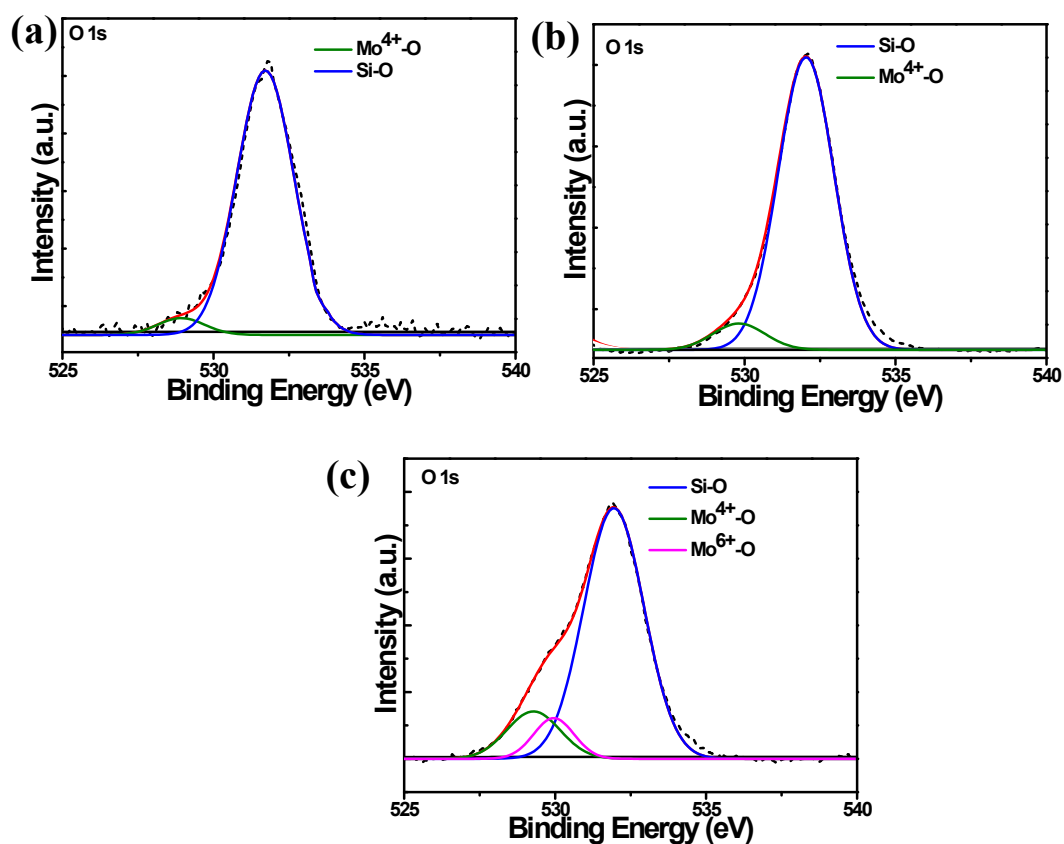


**Figure S3.** XPS O1s core level spectra of as-synthesized MoS<sub>2(1-x)</sub>Se<sub>2x</sub> alloys for substrates A, B, and C, respectively.

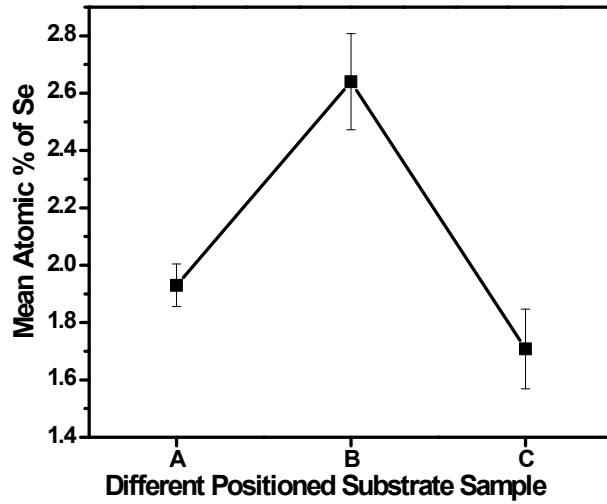


**Figure S4.** Atomic percentage of Se with error bar for each of as-synthesized  $\text{MoS}_{2(1-x)}\text{Se}_{2x}$  alloys on different positioned substrates A, B, and C, respectively.

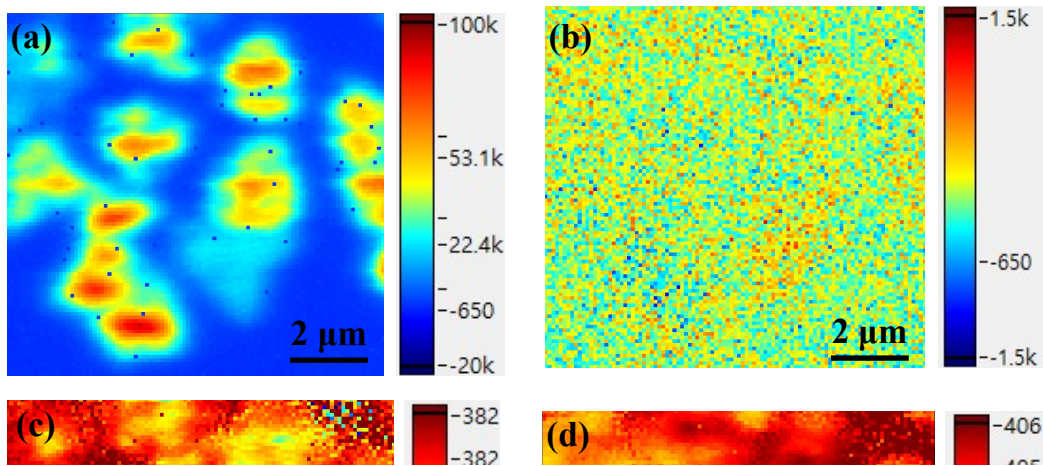


**Figure S 4.** Error bar calculation for each XPS measurements of Se 3d core level spectra of as-synthesized  $\text{MoS}_{2(1-x)}\text{Se}_{2x}$  alloys for substrates A, B, and C, respectively.

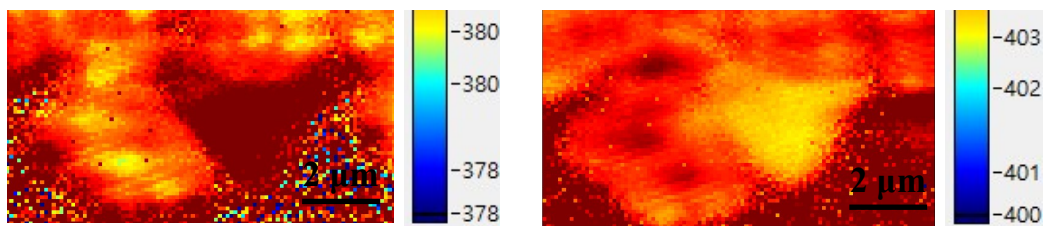


**Figure S5.** (a), (b) Raman intensity map of the  $A_{1g}$  ( $403 \text{ cm}^{-1}$ ) Raman active mode of  $\text{MoS}_2$  and the  $E'_{2g}$  ( $267 \text{ cm}^{-1}$ ) Raman active mode of  $\text{MoSe}_2$  in the  $\text{MoS}_{2(1-x)}\text{Se}_{2x}$  alloy; and (c), (d) position maps of the  $E'_{2g}$  and  $A_{1g}$  active modes of  $\text{MoS}_2$  in the  $\text{MoS}_{2(1-x)}\text{Se}_{2x}$  alloy grown on substrate B.

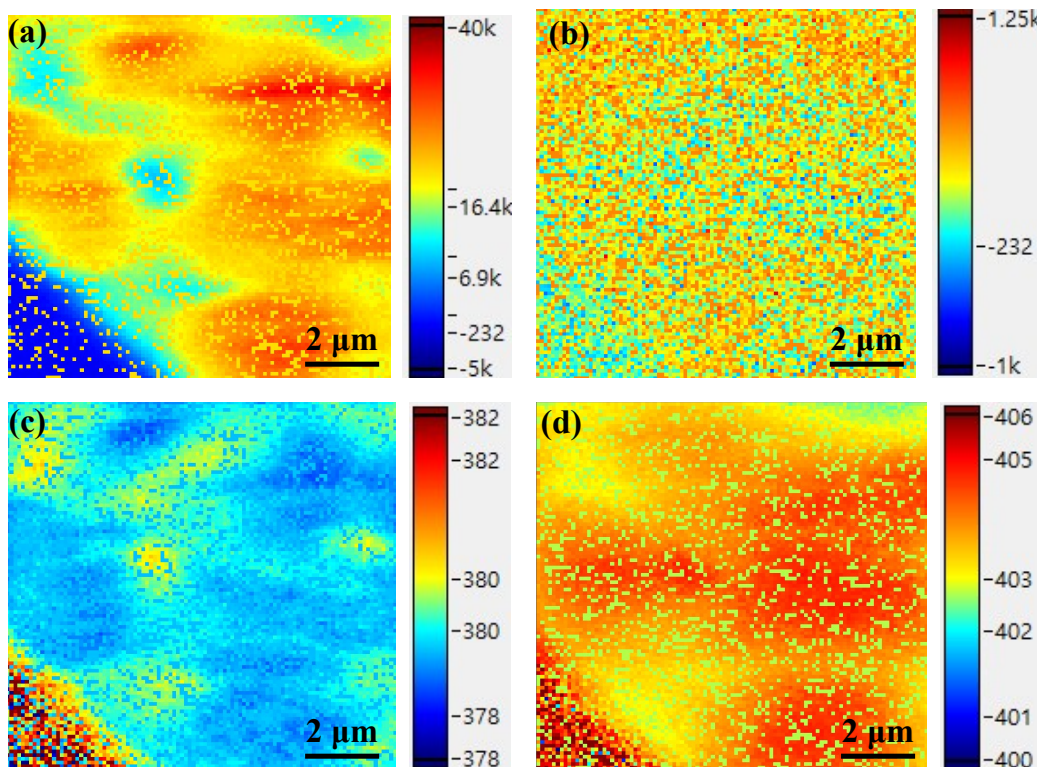


**Figure S6.** (a), (b) Raman intensity map of the  $A_{1g}$  ( $403\text{ cm}^{-1}$ ) Raman active mode of  $\text{MoS}_2$  and the  $E_{2g}^1$  ( $267\text{ cm}^{-1}$ ) Raman active mode of  $\text{MoSe}_2$  in the  $\text{MoS}_{2(1-x)}\text{Se}_{2x}$  alloy; and (c), and (d) position maps of the  $E_{2g}^1$  and  $A_{1g}$  active modes of  $\text{MoS}_2$  in the  $\text{MoS}_{2(1-x)}\text{Se}_{2x}$  alloy grown on substrate A.

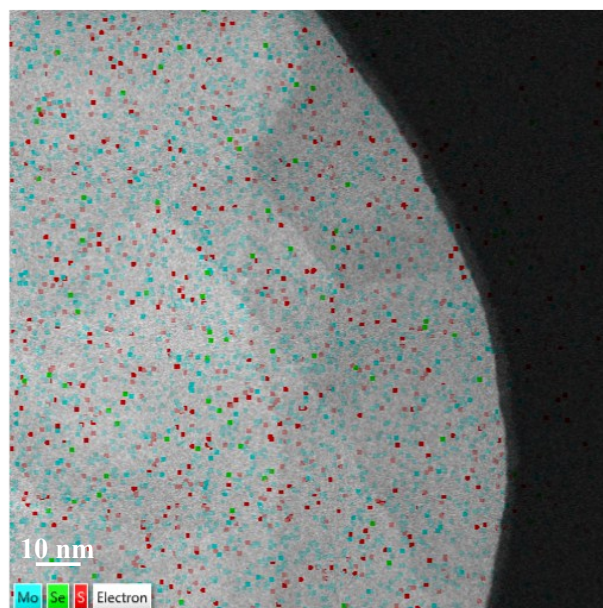


**Figure S7.** EDS map of the  $\text{MoS}_{2(1-x)}\text{Se}_{2x}$  alloy.

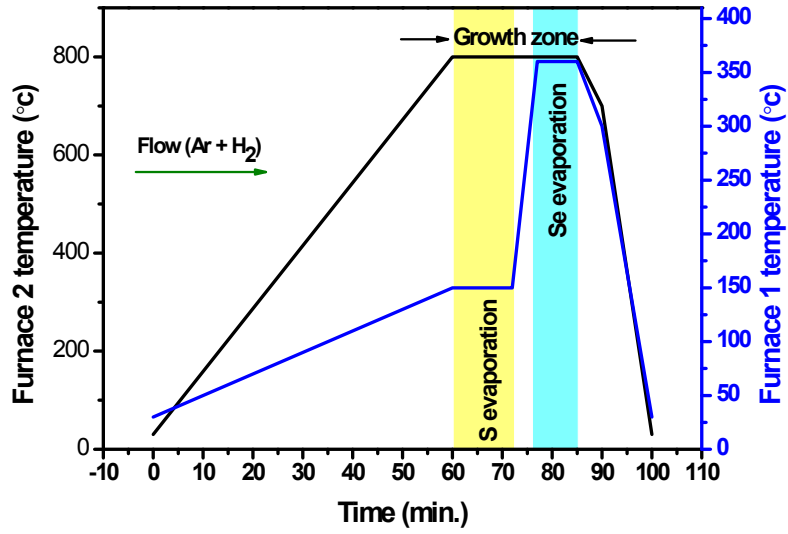


Figure S8. Furnace condition for  $\text{MoS}_{2(1-x)}\text{Se}_{2x}$  alloy growth.

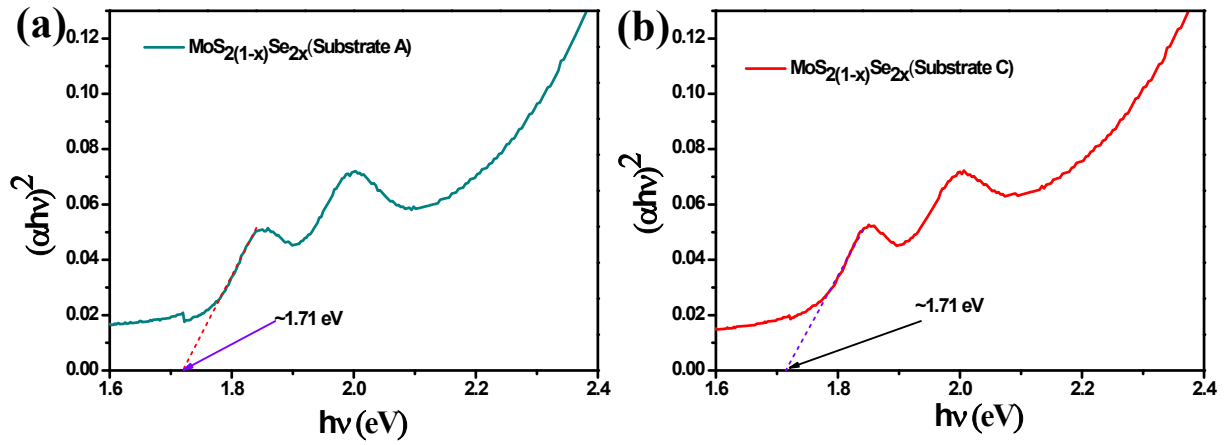


Figure S9. (a) & (b) Tauc's plot to calculate band gap for the  $\text{MoS}_{2(1-x)}\text{Se}_{2x}$  alloy of different position substrate.

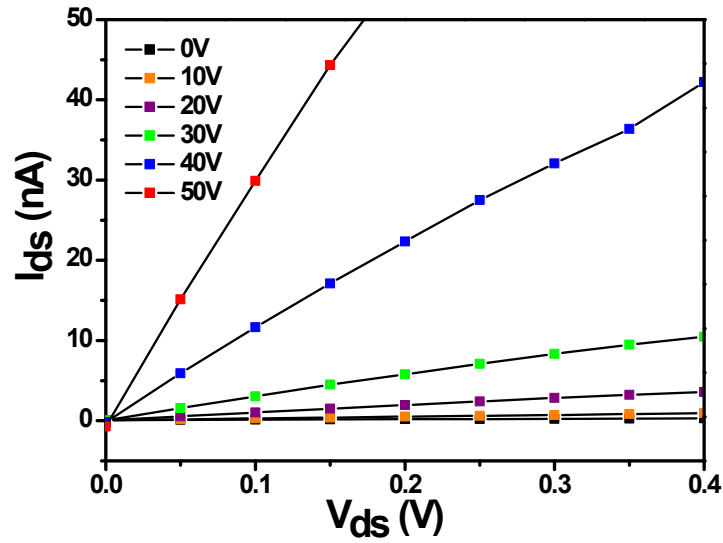


Figure S10. MoS<sub>2(1-x)</sub>Se<sub>2x</sub> FET:  $I_d - V_d$  curve under various  $V_g$  (10 V-50 V).

#### References:

- (S1) J. P. Hirth, G. M. Pound, *Condensation and Evaporation: Nucleation and Growth Kinetics; Progress in materials science*; Macmillan, ISSN 0079-6425, 1963.
- (S2) D. M. Dobkin, M. K. Zuraw, Principles of Chemical Vapor Deposition. *In Springer Netherlands*, 2003; ISBN: 978-990-481-6277-2.
- (S3) A. Baskaran, Smereka, P. *J. Appl. Phys.* **2012**, *111* (4), 044321.
- (S4) P. A. Spevack and N. S. McIntyre, *The Journal of Physical Chemistry*, 1993, **97**, 11031-11036.